Effects of chemical pressure on the Fermi surface and band dispersion of the electron-doped high-T_c superconductors

M. Ikeda,[1] T. Yoshida,[1] A. Fujimori,[1] M. Kubota,[2] K. Ono,[2] Hena Das,[3] T. Saha-Dasgupta,[3] K. Unozawa,[4] Y. Kaga,[4] T. Sasagawa,[4,5] and H. Takagi[4]

[1]*Department of Physics and Department of Complexity Science and Engineering, University of Tokyo, Hongo 7-3-1, Bunkyo-ku, Tokyo 113-0033, Japan*

[2]*Institute of Material Structures Science, High Energy Accelerator Research Organization (KEK), Oho 1-1, Tsukuba, Ibaraki 305-0801, Japan*

[3]*S. N. Bose National Centre for Basic Science, JD Block, Sector 3, Salt Lake City, Kolkata 700098, India*

[4]*Department of Advanced Materials Science, University of Tokyo, Kashiwanoha 5-1-5, Kashiwa, Chiba 277-8561, Japan*

[5]*Materials and Structures Laboratory, Tokyo Institute of Technology, Nagatsuta 4259, Midori-ku, Yokohama, Kanagawa 226-8503, Japan*

(Received 30 October 2008; revised manuscript received 7 June 2009; published 14 July 2009)

We have performed angle-resolved photoemission spectroscopy measurements and first-principles electronic-structure calculations on the electron-doped high-T_c superconductors (HTSCs) $Ln_{1.85}Ce_{0.15}CuO_4$ (Ln=Nd, Sm, and Eu). The observed Fermi surface and band dispersion show such changes that with decreasing ionic size of Ln^{3+} (increasing chemical pressure), the curvature of the Fermi surface or $-t'/t$ decreases, where t and t' are transfer integrals between the nearest-neighbor and next-nearest-neighbor Cu sites, respectively, explaining the apparently inconsistent behavior seen in the hole-doped HTSC $La_{2-x}Sr_xCuO_4$ under epitaxial strain. Around the node, the antiferromagnetic gap is opened with increasing chemical pressure. We propose that the nodal gap opening is possibly due to the decrease in $-t'/t$ through the improved nesting, leading to the decrease in T_c.

DOI: 10.1103/PhysRevB.80.014510 PACS number(s): 74.72.Jt, 74.25.Jb, 74.62.Fj, 79.60.−i

I. INTRODUCTION

Since the discovery of the high-T_c superconductors (HTSCs),[1] a large number of studies have been performed in order to obtain higher critical temperatures. Among them, pressure effects have attracted much attention because it causes a dramatic increase in T_c in many systems. For example, in $HgBa_2Ca_2Cu_3O_4$, which has the highest T_c among HTSCs, T_c rises from 135 to 164 K in a hydrostatic pressure.[2] In addition to mechanical pressure,[3–7] the effect of epitaxial strain in thin films grown on single crystalline substrates,[8–10] and the effect of "chemical pressure," where the lattice constants are varied through substitution of ions with different ionic radii,[11–13] have been studied so far. The effects of epitaxial strain and chemical pressure on T_c are consistent with the mechanical pressure in many cases[3–10] but the mechanism of the T_c changes has not been understood yet. Also, differences in T_c between different cuprate families are expected to provide crucial information about the mechanism of high-T_c superconductivity and have been discussed extensively.[14–17] According to first-principles calculations, the shape of the Fermi surface strongly depends on the distance $d_{\text{Cu-Oap}}$ between the copper and the apical oxygen. A long $d_{\text{Cu-Oap}}$ leads to a strong curvature of the Fermi surface, namely, a large value of $-t'/t$,[14] where t and t' denote transfer integrals between the nearest-neighbor and next-nearest-neighbor Cu sites, respectively, in the single-band tight-binding model. However, the angle-resolved photoemission spectroscopy (ARPES) results of $La_{2-x}Sr_xCuO_4$ (LSCO) under epitaxial strain have demonstrated that compressed in-plane lattice constant and hence increased $d_{\text{Cu-Oap}}$ resulted in a decrease in $-t'/t$,[18,19] contrary to the material dependence of $-t'/t$.[14] That is, the relationship between the crystal structure and the electronic structure of cuprates appears to be more complicated.

In order to clarify the above issues, we have focused on the electron-doped HTSCs $Ln_{2-x}Ce_xCuO_4$ (Ln=Nd, Sm, and Eu), where with decreasing ionic radius of Ln^{3+} from Ln=Nd to Eu, chemical pressure increases, that is, both in-plane and out-of-plane lattice constants become small.[11,12] Since these materials have no apical oxygen, the shape of the Fermi surface is not related to the $d_{\text{Cu-Oap}}$ but determined by other contributions such as the in-plane lattice constant. With increasing chemical pressure, the T_c of this system decreases.[11,13] In addition, the system shows systematic changes in the $x-T$ phase diagram as follows. With increasing chemical pressure, the superconducting phase shrinks[20,21] and the antiferromagnetic phase expands to the higher doping levels.[22–24] Particularly, in $Sm_{2-x}Ce_xCuO_4$, there is a region where the superconducting phase and antiferromagnetic phase coexist around x=0.15. The systematic change in antiferromagnetic phase in this system may suggest that the effect of antiferromagnetism becomes strong with chemical pressure. However, it is not clear why this system shows the systematic changes in antiferromagnetism. Therefore, it is highly desired to investigate the electronic structure of the $Ln_{2-x}Ce_xCuO_4$ by ARPES.

In this paper, we report on an ARPES study and first-principles electronic-structure calculations for the electron-doped HTSCs $Ln_{2-x}Ce_xCuO_4$ (Ln=Nd, Sm, and Eu). The present results show that chemical pressure reduces the curvature of the Fermi surface as in the case of the ARPES results on LSCO thin films.[18] Further analysis of the band dispersions has revealed that the increase in t as a result of the decrease in the in-plane lattice constant has a significant effect on the Fermi-surface shape. From these results associ-

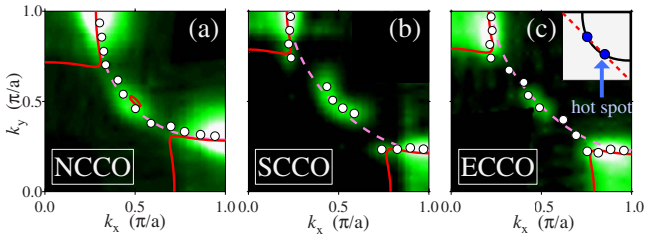

FIG. 1. (Color online) ARPES intensity within ±30 meV of the Fermi level (E_F) plotted in momentum space for (a) NCCO, (b) SCCO, and (c) ECCO. The data were taken over a Brillouin-zone octant and symmetrized with respect to the $(0,0)$-(π,π) line. White circles show the peak positions of MDCs at E_F, indicating the shape of the Fermi surface or underlying Fermi surface. Solid red curves and dashed pink curves show the Fermi surface obtained by tight-binding fit to the ARPES data assuming the paramagnetic and antiferromagnetic band structures, respectively. Inset: schematic diagram of the hot spot. A black curve and a red dashed line represent the Fermi surface and the antiferromagnetic Brillouin-zone boundary, respectively. The intersecting points of them are hot spots as shown by blue circles.

ated with T_c variation, we suggest the empirical relationship between $-t'/t$ and T_c for the electron-doped HTSCs. Also, around the node the opening of the antiferromagnetic gap was observed with chemical pressure. We shall discuss the superconductivity from the systematic change in this antiferromagnetic gap and $-t'/t$.

II. EXPERIMENT

High-quality single crystals of optimally doped $Nd_{1.85}Ce_{0.15}CuO_4$ (NCCO), $Sm_{1.85}Ce_{0.15}CuO_4$ (SCCO), and $Eu_{1.85}Ce_{0.15}CuO_4$ (ECCO) were grown by the traveling solvent floating-zone method. The T_c's of NCCO, SCCO, and ECCO were ~22, ~16, and 0 K, respectively. There was slight deviation in the Ce content and/or the oxygen stoichiometry from the indicated composition, as reflected on small differences in the Fermi-surface areas among NCCO, SCCO, and ECCO. The ARPES measurements were performed at beamline 28 A of Photon Factory, Institute of Materials Structure Science, High Energy Accelerators Research Organization (KEK), using incident photons with energy of 55 eV, at which the band dispersion is clearly observed.[25] We used a SCIENTA SES-2002 electron-energy analyzer (acceptance angle ~15°) in the angle mode, and used a five-axis manipulator.[26] We cleaved the samples *in situ*. The incident angle of photons changed from 45° to 25° to the sample surface. The total-energy resolution and momentum resolution were 15 meV and 0.2°, respectively, and samples were measured at ~10 K. The Fermi edge of gold was used to determine the Fermi-level (E_F) position and the instrumental resolution before and after the ARPES measurements.

III. RESULTS AND DISCUSSION

Figure 1 shows plots of ARPES intensity at E_F in NCCO, SCCO, and ECCO in two-dimensional momentum space. The suppression of the intensity is seen near the "hot spots," i.e., the intersecting points of the paramagnetic Fermi surface and the antiferromagnetic Brillouin-zone boundary [see the inset in Fig. 1(c)]. This suppression is due to the scattering of electrons at E_F by antiferromagnetic fluctuations or by (quasi)static antiferromagnetic correlation with wave vector (π,π) as discussed in previous ARPES studies.[25,27] Around $(\pi,0)$, one can see that the intensity becomes strong in going from NCCO to ECCO. Since the appearance of the intensity in this region is due to a shadow band whose origin is the effect of antiferromagnetism, the results indicate that the effect of antiferromagnetism becomes strong in going from NCCO to ECCO, consistent with the results indicated by the $x-T$ phase diagram.[22–24] White circles in Fig. 1 represent the peak positions of the momentum distribution curves (MDCs) at E_F and represent the Fermi surface or remnant Fermi surface. As seen from Fig. 1, the curvature of the Fermi surface in NCCO is the strongest among the three materials.

We quantitatively evaluated the difference of the curvature among the three compounds using a tight-binding model as follows. We used two-dimensional antiferromagnetic tight-binding model,

$$\epsilon - \mu = \varepsilon_0 \pm \sqrt{\Delta E^2 + 4t^2(\cos k_x a + \cos k_y a)^2} - 4t' \cos k_x a \cos k_y a - 2t''(\cos 2k_x a + \cos 2k_y a),$$

where t, t', and t'' are transfer integrals between the nearest-neighbor, second-nearest-neighbor, and third-nearest-neighbor Cu sites, respectively, ε_0 represents the center of the band relative to the chemical potential μ, and $2\Delta E$ is the potential-energy difference between the spin-up and spin-down sublattices.

First, we fitted the calculated Fermi surface to the set of white circles in Fig. 1 by adjusting the parameters $-t'/t$ and $-\varepsilon_0/t$. We note that the curvature of the Fermi surface depends on the ratio $-t'/t$ and not on each of t and t', and only very weakly on $-\varepsilon_0/t$. Assuming that $-t''/t'=0.50$, we obtained $-t'/t=0.20$, 0.12, and 0.11 for NCCO, SCCO, and ECCO, respectively, and $\varepsilon_0/t=-0.12$, 0, and -0.05 for NCCO, SCCO, and ECCO, respectively. The Fermi-surface area was allowed to deviate slightly from what is expected for 15% Ce doping because of nonstoichiometry. Note that when we performed the same analysis retaining only the second-nearest-neighbor Cu hopping ($t''=0$), we obtained $-t'/t=0.40$, 0.23, and 0.21 for NCCO, SCCO, and ECCO, respectively, showing a similar tendency to the case of $-t''/t'=0.50$. The present fitted results demonstrate that the curvature of the Fermi surface monotonically decreases from NCCO to SCCO to ECCO.

Next, we evaluated the absolute values of t and t' by fitting the calculated band dispersion to the MDC and/or energy-distribution-curve (EDC) peak positions with $-t'/t$ and $-\varepsilon_0/t$ fixed at the above values. Because the position of the "flat band" at $\sim(\pi,0)$ is sensitive to $-t'$, it can be used to determine t' and t separately. Figure 2 shows the $E-k$ plot of ARPES intensity for NCCO, SCCO, and ECCO along two different cuts as shown in the inset. Panels (d)–(f) show that the position of the band around the $(\pi,0)$ point becomes shallower in going from NCCO to ECCO, indicating that $-t'$ decreases. As a result, we obtained $t=0.27$, 0.30, and 0.32 for

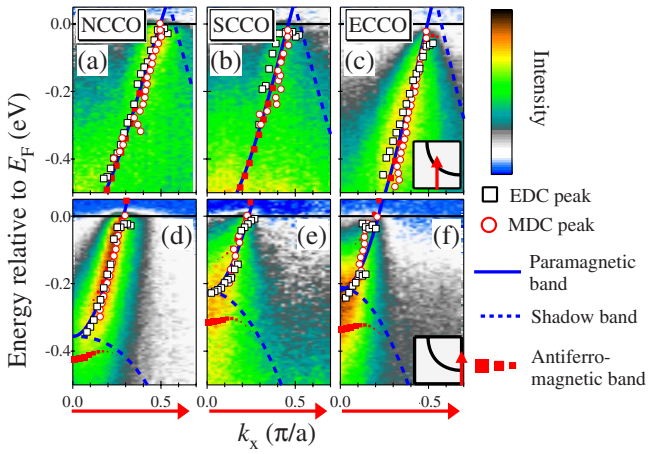

FIG. 2. (Color online) ARPES intensity plot in energy-momentum space in the nodal and antinodal regions of the Brillouin zone compared with tight-binding energy bands. (a) and (d): NCCO; (b) and (e): SCCO; and (c) and (f): ECCO. The cuts are shown in the inset. The direction of the cut is shown in the inset. Squares and circles denote EDC peak positions and MDC peak positions, respectively. Blue solid curves and blue dotted curves represent the paramagnetic energy band and shadow band, respectively, obtained by the tight-binding analysis. The spectral intensity of the antiferromagnetic band is represented by the size of red squares.

NCCO, SCCO, and ECCO, respectively, and ΔE=0.07, 0.09, and 0.11 for NCCO, SCCO, and ECCO, respectively. In the indication of antiferromagnetic tight-binding bands with the above parameters, we have assumed that the spectral intensity is proportional to the projected weight of the antiferromagnetic band to the paramagnetic band. We have presented the spectral intensity by the size of the point as shown in Fig. 2. In the nodal region [panels (a)–(c)] the experimental band dispersion as well as spectral weight is well explained by the antiferromagnetic band while around the $(\pi,0)$ region [panels (d)–(f)], the experimental one cannot be explained by the antiferromagnetic band well but rather by the paramagnetic band (ΔE=0). These fitting results may indicate that the k dependence of the antiferromagnetic gap ΔE exists beyond standard band theory of the antiferromagnetic state, as predicted by a recent variational Monte Carlo study.[28]

In Fig. 3, we present EDCs in the nodal direction for NCCO, SCCO, and ECCO. The EDCs at the Fermi momentum for these materials are superposed in Fig. 3(d). A leading edge (LE) shift, which is the indication of the gap, is observed for SCCO (LE shift: ~5 meV), consistent with a recent ARPES study on $Sm_{1.86}Ce_{0.14}CuO_4$,[29] and for ECCO (LE shift: ~30 meV), but not observed for NCCO, indicating an increase in the effect of antiferromagnetism in going from NCCO to ECCO. Considering the variation in T_c of these materials, the results suggest the competition between superconductivity and antiferromagnetism. Note that the systematic variation in the effect of antiferromagnetism is evaluated from the tight-binding analysis through the increase in ΔE as shown in Fig. 4. The increase in ΔE may result from the increase in the antiferromagnetic interaction between Cu sites J caused by the increase in t through $J=4t^2/U$.

In order to see the effect of chemical pressure on the band structure from first-principles calculation, we have carried

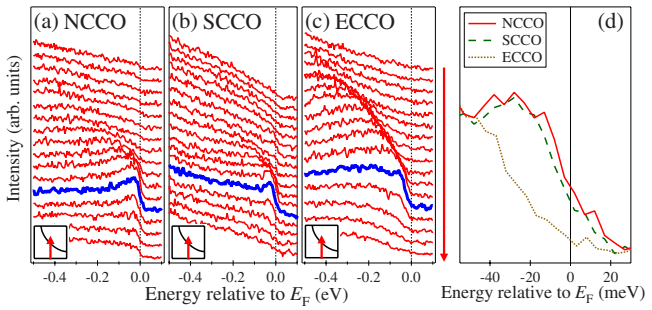

FIG. 3. (Color online) EDCs for (a) NCCO, (b) SCCO, and (c) ECCO around the nodal k_F point. Blue thick EDCs represent EDCs at k_F. The direction of the cut is shown in the insets. (d) EDCs of NCCO, SCCO, and ECCO at the nodal k_F point.

out muffin-tin-orbital (MTO)-based N-MTO calculations[30] within the framework of local-density approximation (LDA) and extracted the transfer integrals corresponding to t, t', and t'' in the tight-binding model. For this purpose, an effective Cu $d_{x^2-y^2}$ basis was defined by means of the downfolding procedure, by integrating out all the degrees of freedom related to Ln, O, and Cu except for Cu $d_{x^2-y^2}$. The effective basis, constructed in this manner, serves the purpose of the Wannier-type function corresponding to the single band crossing the E_F. The real-space Hamiltonian defined in the basis of these effective, Wannier-type orbitals provides the information about the various transfer integrals, connecting various Cu sites. This method has been applied successfully in the case of hole-doped cuprate compounds.[14] Calculations have been carried out for Ln=Nd and Sm. The calculated band structure for Ln=Nd and Sm are shown in Figs. 5(a) and 5(b), respectively. Wannier-type function corresponding to LDA conduction band projected in Cu-O plane are shown in lower panels in Fig. 5. The central part of the function has the Cu $d_{x^2-y^2}$ symmetry while the tails are shaped according to integrated out orbitals such as O-p, Cu-d orbitals other than Cu $d_{x^2-y^2}$ and Nd/Sm orbitals. From the above calculation, $-t'/t$ turned out to be 0.34 (t=0.41 eV and t'

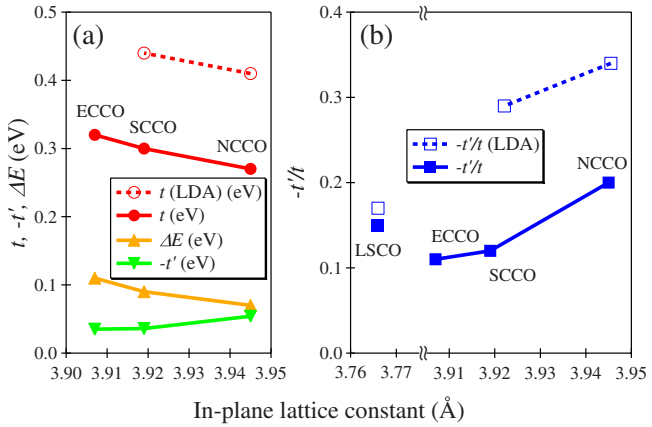

FIG. 4. (Color online) [(a) and (b)]: tight-binding parameters as functions of in-plane lattice constant. As the in-plane lattice constant decreases, $-t'$ and $-t'/t$ decreases while t and ΔE increase. Dashed lines are results from the LDA calculations. LSCO data are taken from Refs. 14 and 32.

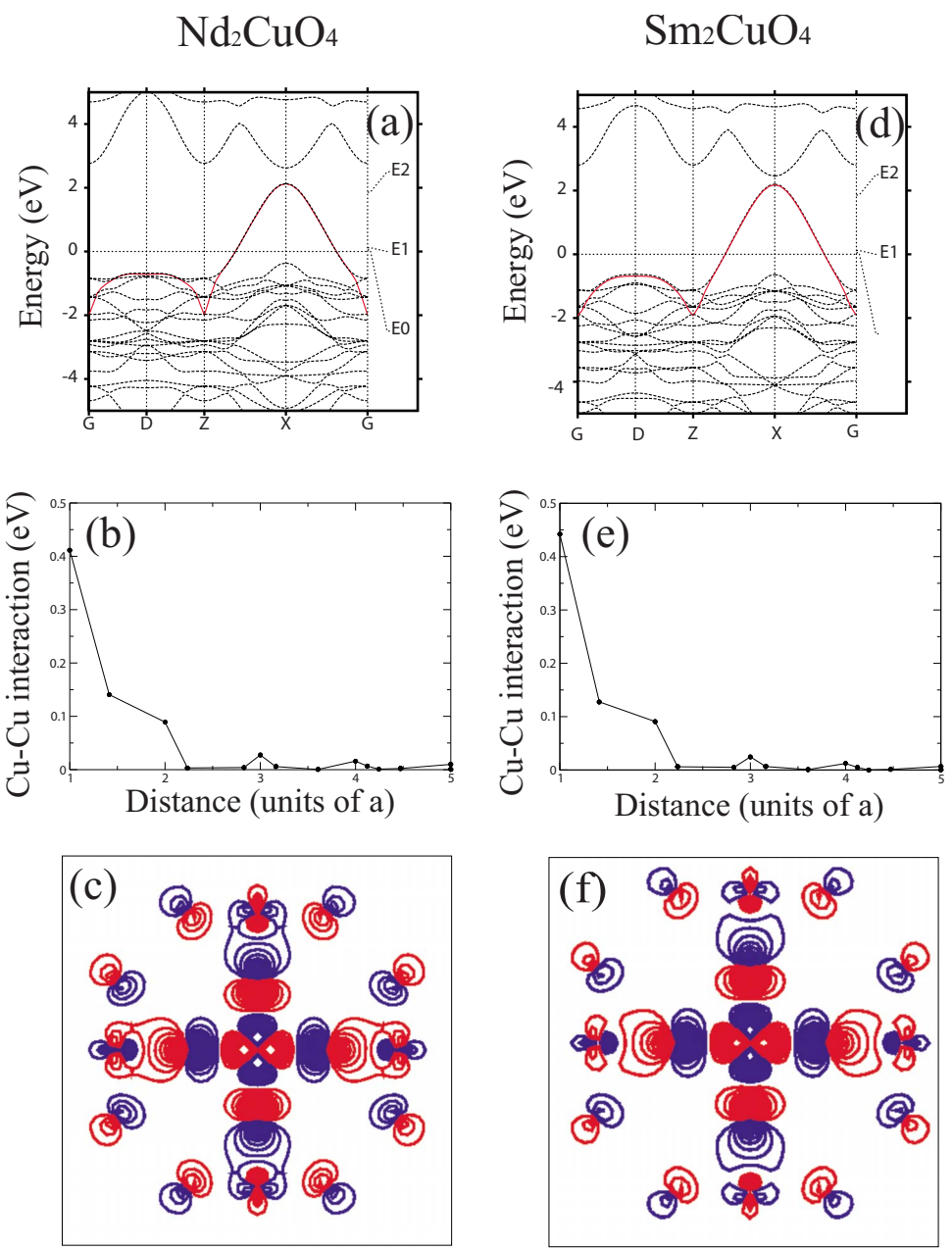

FIG. 5. (Color online) Upper panels: LDA band structure (in dotted lines) of Nd_2CuO_4 and Sm_2CuO_4 in comparison with downfolded one band (in red solid lines). Middle panels: computed Cu-Cu hopping interactions plotted as a function of Cu-Cu distance in units of in-plane lattice constant a (=3.94 Å for Nd_2CuO_4 and =3.91 Å for Sm_2CuO_4). Lower panels: Wannier-type function corresponding to LDA conduction band projected in Cu-O plane. The central part of the function has the Cu $d_{x^2-y^2}$ symmetry while the tails are shaped according to integrated out orbitals such as O-p, Cu-d orbitals other than Cu $d_{x^2-y^2}$ and Nd/Sm orbitals. Red and blue colors correspond to two differently signed lobes of the orbitals.

=−0.14 eV) for NCCO and 0.29 (t=0.44 eV and t' =−0.13 eV) for SCCO, quantitatively consistent with the experimental results as shown in Fig. 4. Moderate change in $-t'/t$, compared with the hole-doped cuprate family is expected considering the absence of apical oxygen in the T' structure, one of the key controlling factor in determining $-t'/t$.[14] Also, according to cellular dynamical mean-field theory,[31] $-t'/t$ is reduced by electron correlation over the LDA estimate for electron-doped cuprates and increased for hole-doped systems, with the effect being strong for electron-doped case at low doping level. This may explain the disparity in the quantitative values of $-t'/t$ as seen in Fig. 4, where for LSCO a good agreement in $-t'/t$ between the LDA and the experimental estimate was observed.

Considering the nearest-neighbor Cu-Cu transfer integral t to be given by the relationship $t=2(t_{pd})^2/(\varepsilon_d-\varepsilon_p)$, where t_{pd} and $\varepsilon_d-\varepsilon_p$ are the Cu 3d-O 2p transfer integral and the on-site energy differences, respectively, defined within the three band model, the increase in t in going from Nd to Sm is contributed both by the increase in t_{pd} due to contraction of the lattice, as well as due to decrease in $(\varepsilon_d-\varepsilon_p)$ caused by the replacement of Nd by Sm. Our NMTO-downfolding calculations keeping oxygen-$p\sigma$ degrees of freedom active in addition to Cu $d_{x^2-y^2}$ gives a 8% change in t_{pd} while the rest is contributed by the change in $(\varepsilon_d-\varepsilon_p)$. The decrease of the second-nearest-neighbor hopping, t' in moving from Nd to Sm is, on the other hand, contributed by the decrease in the O-O hopping, t_{pp} as obtained in our two-band calculations, presumably caused by the different cation covalency effect between Nd and Sm.

We now turn our attention to the case of strained LSCO thin films. In LSCO, the reduced in-plane lattice constant by compressive strain lead to the decrease in $-t'/t$,[18] as in the present electron-doped system. Hence, the experimental re-

sults indicate that the reduced in-plane lattice constant resulted in the reduced value of $-t'/t$ both under chemical pressure and epitaxial strain and both for the hole-doped and electron-doped compounds. Also, since the electron-doped HTSCs have no apical oxygen, the shape of the Fermi surface in our experiment is not related to $d_{\text{Cu-Oap}}$ but is related to the in-plane lattice constant including the effect of O-O hopping. Therefore, we consider that in the strained LSCO film the effects of in-plane lattice constant is stronger than those of $d_{\text{Cu-Oap}}$.

Finally, we discuss the superconductivity from the viewpoint of the systematic change in $-t'/t$ and the antiferromagnetic gap around the node with chemical pressure. In the hole-doped HTSCs, there is an empirical trend that the larger $-t'/t$ is, the higher T_c becomes.[14] The present results on $-t'/t$ in the electron-doped system follow the same trend, but considering the LDA estimates of $-t'/t$, the predicted T_c would be higher, ~90 and ~70 K for NCCO and SCCO, respectively. The gap opening in the nodal direction may explain the generally low T_c's in the electron-doped systems compared with hole-doped ones as well as the systematic suppression of T_c with chemical pressure because electrons near the nodal point significantly contribute to the superconductivity, according to the Raman-scattering studies[33] and variational cluster calculations.[34] In addition, in going from NCCO to ECCO, the compression of the out-of-plane lattice constant becomes strong compared with that of the in-plane lattice constant.[11] The decrease in the interlayer distance may cause the development of the three-dimensional antiferromagnetic order, leading to the large antiferromagnetic gap around the node. One may consider that since $-t'/t$ of SCCO is closer to that of ECCO than that of NCCO, the effect of $-t'/t$ is not important for superconductivity. Indeed, as shown in Fig. 3(d), the size of the antiferromagnetic gap rather than $-t'/t$ is likely to be more intimately connected with T_c. However, it is also important to note that the reduced $-t'/t$ enhances the effect of antiferromagnetism through strengthened nesting, resulting in the increased gap in the nodal region. As for the hole-doped HTSCs, it has been argued that the relationship between $-t'/t$ and T_c is caused by the enhancement of stripelike antiferromagnetic fluctuations for small $-t'/t$.

IV. CONCLUSION

In conclusion, we have performed ARPES and first-principles electronic-structure calculation studies of NCCO, SCCO, and ECCO in order to elucidate the variation in electronic structure by chemical pressure. As the in-plane lattice constant decreases, $-t'/t$ decreases and t increases, consistent with the previous ARPES results on strained LSCO films. This suggests that the variation in the in-plane lattice constant has a great influence on the electronic structures. We consider that the decrease in T_c with increasing chemical pressure is attributed to the antiferromagnetic gap opening near the nodal point possibly through the change in the Fermi surface.

ACKNOWLEDGMENTS

We are grateful to T. Tohyama, T. K. Lee, C. M. Ho, C. P. Chou, N. Nagaosa, and N. Bontemps for enlightening discussion. This work was done under the approval of the Photon Factory Program Advisory Committee (Proposal No. 2006S2-001) and was supported by a Grant-in-Aid for Scientific Research in Priority Area "Invention of Anomalous Quantum Materials" from the Ministry of Education, Culture, Sports, Science, and Technology, Japan. We also thank the Material Design and Characterization Laboratory, Institute for Solid State Physics, University of Tokyo, for the use of the SQUID magnetometer.

[1] J. G. Bednorz and K. A. Müller, Z. Phys. B **64**, 189 (1986).
[2] L. Gao, Y. Y. Xue, F. Chen, Q. Xiong, R. L. Meng, D. Ramirez, C. W. Chu, J. H. Eggert, and H. K. Mao, Phys. Rev. B **50**, 4260 (1994).
[3] X. Chen, G. X. Tessema, and M. J. Skove, Physica C **181**, 340 (1991).
[4] F. Gugenberger, C. Meingast, G. Roth, K. Grube, V. Breit, T. Weber, H. Wuhl, S. Uchida, and Y. Nakamura, Phys. Rev. B **49**, 13137 (1994).
[5] M. Nohara, T. Suzuki, Y. Maeno, T. Fujita, I. Tanaka, and H. Kojima, Phys. Rev. B **52**, 570 (1995).
[6] C. Meingast, A. Junod, and E. Walker, Physica C **272**, 106 (1996).
[7] F. Nakamura, T. Goko, J. Hori, Y. Uno, N. Kikugawa, and T. Fujita, Phys. Rev. B **61**, 107 (2000).
[8] J.-P. Locquet, Y. Jaccard, A. Cretton, E. J. Williams, F. Arrouy, E. Machler, T. Schneider, O. Fischer, and P. Martinoli, Phys. Rev. B **54**, 7481 (1996).
[9] H. Sato and M. Naito, Physica C **274**, 221 (1997).
[10] J.-P. Locquet, J. Perret, J. Fompeyrine, E. Machler, J. W. Seo, and G. V. Tendeloo, Nature (London) **394**, 453 (1998).
[11] J. T. Markert, J. Beille, J. J. Neumeier, E. A. Early, C. L. Seaman, T. Moran, and M. B. Maple, Phys. Rev. Lett. **64**, 80 (1990).
[12] T. Uzumaki, N. Kamehara, and K. Niwa, Jpn. J. Appl. Phys. **30**, L981 (1991).
[13] M. Naito and M. Hepp, Jpn. J. Appl. Phys. **39**, L485 (2000).
[14] E. Pavarini, I. Dasgupta, T. Saha-Dasgupta, O. Jepsen, and O. K. Andersen, Phys. Rev. Lett. **87**, 047003 (2001).
[15] K. Tanaka, T. Yoshida, A. Fujimori, D. H. Lu, Z.-X. Shen, X.-J. Zhou, H. Eisaki, Z. Hussain, S. Uchida, Y. Aiura, K. Ono, T. Sugaya, T. Mizuno, and I. Terasaki, Phys. Rev. B **70**, 092503 (2004).
[16] V. Gavrichkov, A. Borisov, and S. G. Ovchinnikov, Phys. Rev. B **64**, 235124 (2001).
[17] C. Janowitz, U. Seidel, R.-ST. Unger, A. Krapf, R. Manzke, V. A. Gavrichkov, and S. G.Ovchinnikov, arXiv:cond-mat/0411406 (unpublished).
[18] M. Abrecht, D. Ariosa, D. Clotta, S. Mitrovic, M. Onellion, X. X. Xi, G. Margaritondo, and D. Pavuna, Phys. Rev. Lett. **91**,

057002 (2003).
[19] D. Cloetta, D. Ariosa, C. Cancellieri, M. Abrecht, S. Mitrovic, and D. Pavuna, Phys. Rev. B **74**, 014519 (2006).
[20] A. Tsukada, Y. Krockenberger, M. Noda, H. Yamamoto, D. Manskeb, M. Naito, and L. Alff, Solid State Commun. **133**, 427 (2005).
[21] Y. Krockenberger, J. Kurian, A. Winkler, A. Tsukada, M. Naito, and L. Alff, Phys. Rev. B **77**, 060505(R) (2008).
[22] T. Kubo, T. Uefuji, M. Fujita, K. Yamada, I. Watanabe, and K. Nagamine, Physica C **378-381**, 354 (2002).
[23] M. Fujita, T. Kubo, S. Kuroshima, T. Uefuji, K. Kawashima, K. Yamada, I. Watanabe, and K. Nagamine, Phys. Rev. B **67**, 014514 (2003).
[24] T. Sasagawa, K. Unozawa, K. Ohishi, S. Pyon, K. H. Satoh, A. Koda, R. Kadono, and H. Takagi, KEK-MSL Progress Report 2005 (2006), p. 13.
[25] N. P. Armitage, D. H. Lu, C. Kim, A. Damascelli, K. M. Shen, F. Ronning, D. L. Feng, P. Bogdanov, Z.-X. Shen, Y. Onose, Y. Taguchi, Y. Tokura, P. K. Mang, N. Kaneko, and M. Greven, Phys. Rev. Lett. **87**, 147003 (2001).
[26] Y. Aiura, H. Bando, T. Miyamoto, A. Chiba, R. Kitagawa, S. Maruyama, and Y. Nishihara, Rev. Sci. Instrum. **74**, 3177 (2003).
[27] H. Matsui, K. Terashima, T. Sato, T. Takahashi, S.-C. Wang, H.-B. Yang, H. Ding, T. Uefuji, and K. Yamada, Phys. Rev. Lett. **94**, 047005 (2005).
[28] C. P. Chou and T. K. Lee, J. Phys. Chem. Solids **69**, 2944 (2008).
[29] S. R. Park, Y. S. Roh, Y. K. Yoon, C. S. Leem, J. H. Kim, B. J. Kim, H. Koh, H. Eisaki, N. P. Armitage, and C. Kim, Phys. Rev. B **75**, 060501(R) (2007).
[30] O. K. Andersen and T. Saha-Dasgupta, Phys. Rev. B **62**, R16219 (2000).
[31] M. Civelli, M. Capone, S. S. Kancharla, O. Parcollet, and G. Kotliar, Phys. Rev. Lett. **95**, 106402 (2005).
[32] T. Yoshida, X. J. Zhou, K. Tanaka, W. L. Yang, Z. Hussain, Z.-X. Shen, A. Fujimori, S. Sahrakorpi, M. Lindroos, R. S. Markiewicz, A. Bansil, S. Komiya, Y. Ando, H. Eisaki, T. Kakeshita, and S. Uchida, Phys. Rev. B **74**, 224510 (2006).
[33] M. M. Qazilbash, A. Koitzsch, B. S. Dennis, A. Gozar, Hamza Balci, C. A. Kendziora, R. L. Greene, and G. Blumberg, Phys. Rev. B **72**, 214510 (2005).
[34] M. Aichhorn, E. Arrigoni, M. Potthoff, and W. Hanke, Phys. Rev. B **74**, 024508 (2006).